Defect-mediated ferromagnetism and controlled switching characteristics in ZnO

Siddhartha Mal,[a] Sudhakar Nori, and Jagdish Narayan
Department of Materials Science and Engineering, North Carolina State University, Raleigh, North Carolina 27695

John T. Prater
Materials Science Division, Army Research Office, Research Triangle Park, North Carolina 27709

(Received 21 December 2010; accepted 15 February 2011)

We report a detailed study of the structural, chemical, electrical, and magnetic properties of undoped ZnO thin films grown under different conditions and the films that were annealed in various environments and irradiated with an ultraviolet laser. Samples prepared in low oxygen pressure or subsequently annealed in vacuum have always been strongly magnetic. Oxygen-annealed films displayed a sequential transition from the ferromagnetic to the diamagnetic state as a function of the annealing temperature. Reversible switching of room temperature ferromagnetism and n-type conductivity have been demonstrated either by annealing in different environments or by a novel laser irradiation treatment. Enhancements in both the electrical conductivity and magnetic moment have been controlled precisely with laser pulses, without altering the crystal structure. Electron paramagnetic resonance data were found to be in good agreement with the magnetization and conductivity measurements. Our secondary ion mass spectrometer and electron energy loss spectrometer studies conclusively rule out the presence of any external ferromagnetic impurities.

I. INTRODUCTION

Recent research efforts on the growth of diluted magnetic semiconductors (DMS) exhibiting Curie temperatures above 300 K have received a great attention due to their potential applications in spintronics devices.[1] Following the theoretical prediction of a possible room temperature ferromagnetism (RTFM) in Mn-doped ZnO,[2] studies on transition metal (TM)-doped ZnO system have intensified. RTFM has been reported in Co-,[3] Mn-, Cr-, and Ni[4]-doped ZnO systems. However, similar studies on Co- and Mn-doped polycrystalline ZnO[5] and high quality ZnO:Co[6] thin films grown by pulsed laser deposition (PLD) have not shown any ferromagnetism. Surprisingly, x-ray magnetic circular dichroism studies on Co-doped samples by Gacic et al.[7] showed that magnetism is not induced by the TM dopant atoms, either in solid solution or in the form of clusters or secondary phases. These conflicting results have generated controversy on the origin of observed ferromagnetism and raised questions about the role of dopants. Finally, the observation of RTFM in undoped HfO_2[8] has challenged the understanding of magnetism and triggered researchers to revisit the role of dopants in controlling the magnetism of semiconducting and insulating oxides. Since then this so-called d^0 ferromagnetism has been observed in other systems as well, such as TiO_2, In_2O_3,[9] and nonstoichiometric CaB_6.[10] In case of TiO_2 and HfO_2 systems, the ferromagnetism has been attributed to the presence of oxygen vacancies (V_O).[11] RTFM has also been reported in undoped ZnO powders, nanoparticles, nanorods, nanowires, and thin films.[12–15]

An important but often overlooked aspect of the controversy regarding the observation of ferromagnetism in TM-doped ZnO is related to the role of intrinsic defects, metal precipitates, and TM–defect complexes.[16] However, the ferromagnetism in undoped ZnO is linked to the poor crystalline quality, strain, grain boundaries, and intrinsic defects, namely, V_O, zinc vacancies (V_{Zn}), and zinc interstitials (I_{Zn}). Recent ab initio calculations have suggested that the magnetic moment arises from the unpaired 2p electrons at the O sites surrounding the V_{Zn} with each nearest neighbor O atom carrying a magnetic moment ranging from 0.49 to 0.74 μ_B.[17] Recently, RTFM was induced in undoped ZnO powder by applying a mechanical force[18] and then destroyed upon oxygen annealing. It was suggested in this case that the onset of FM had its origin in the unpaired spin states generated by mechanical strain and/or dislocations at the crystalline domain boundaries.

In our experience, point defects such as V_O, V_{Zn}, and I_{Zn} are always present in the ZnO films grown by PLD and that these intrinsic defects play an important role in tailoring the physical properties of the films. We find that undoped ZnO films can be tailored to be ferromagnetic by invoking nonstoichiometric processing conditions,

[a]Address all correspondence to this author.
e-mail: smal@ncsu.edu
DOI: 10.1557/jmr.2011.74

 © Materials Research Society 2011

https://doi.org/10.1557/jmr.2011.74 Published online by Cambridge University Press

such as low oxygen partial pressure (pO_2) growth, vacuum annealing, and laser irradiation, and further that the magnetization is destroyed upon high temperature oxygen annealing. These observations strongly suggest that the intrinsic point defects play an important role in introducing and controlling ferromagnetism in nominally pure ZnO. The primary focus of this study is to grow high-quality epitaxial single crystal films of pure ZnO on *c*-sapphire and to investigate their ferromagnetic and concomitant electrical and structural properties as a function of pulsed laser irradiation and thermal annealing in different environments. It is shown that these treatments can controllably vary the magnetic and electrical properties of ZnO films, which we infer to be associated with the introduction of defects, particularly V_o and V_{Zn} within the oxide matrix. Here, we report a detailed study of the electrical and magnetic properties of the films grown under different deposition conditions that were further subjected to different postgrowth annealing treatments. With the aid of Hall and electron paramagnetic resonance (EPR) data, the role of defects in modifying the magnetic properties of ZnO films has been illustrated and correlated with the electrical and other structural properties.

II. EXPERIMENTAL DETAILS

ZnO thin films have been deposited on single crystal *c*-plane sapphire substrates using PLD. A KrF excimer laser (λ = 248 nm, τ = 25 ns) with a pulse energy density of 3–4 J/cm^2 at a repetition rate of 10 Hz was used to deposit thin films. The target–substrate distance was maintained at 4.5 cm during the film deposition. A high purity (5N) ZnO target was prepared using the conventional solid state reaction technique. Special care was taken to avoid any TM contamination, e.g., nonmagnetic plastic tweezers were used throughout the sample growth and characterization processes. A series of thin films were deposited for 15 min at substrate temperatures (T_{dep}) ranging from room temperature to 750 °C and under different pO_2 ranging from 10^{-5} to 1 Torr. The deposition chamber was evacuated to a base pressure of less than 1×10^{-6} Torr before the introduction of oxygen. Postdeposition annealing was carried out for 30 min in a high purity oxygen atmosphere at different annealing temperatures from 200 to 800 °C. Vacuum annealing was performed at 10^{-5} Torr for 3 h at 800 °C. Laser irradiation of films was carried out at room temperature in ambient air with a laser energy density of 0.2 J/cm^2 and a frequency of 1 Hz for different numbers of pulses. The laser energy was kept below the threshold for melting, which was easily identified by the formation of cracks in the film. The structure of these films was characterized by x-ray diffraction (XRD) using a x-ray diffractometer (Rigaku Corporation, Tokyo, Japan) with Cu K_α radiation (λ = 0.154 nm) and a Ni filter. Microstructural characterization was carried out using a JEOL-2010 field emission transmission electron microscope (TEM; JEOL, Tokyo, Japan) equipped with a Gatan image filter tuning attachment (Gatan, Pleasanton, CA). The samples were examined by secondary ion mass spectrometer (SIMS) and an electron energy loss spectrometer (EELS) to determine their chemical composition and to assess for the presence of any unintended impurities. X-ray photoelectron spectroscopy (XPS) was performed using a LAS-3000 instrument (Riber, Rueil-Malmaison Cedex, France) with an Mg K_α x-ray source having an energy resolution of 0.9–1.0 eV. Room temperature electrical resistivity measurements were carried out using a four-point probe method, and Hall measurements were performed using an Ecopia Hall measurement system. Magnetic measurements were carried out using a vibrating sample magnetometer in conjunction with a physical property measurement system (Quantum Design Inc., San Diego, CA) and an alternating gradient magnetometer (Princeton Measurements Inc., Princeton, NJ). X-band (~9.5 GHz) EPR spectroscopy measurements in the 4–300 K temperature range were carried out with an ER-200 spectrometer (Bruker, Santa Barbara, CA) equipped with a helium flow cryostat (Oxford Instruments, Concord, MA). The experimental spectra were least squares simulated using Lorentzian line shape models with the help of the EWVOIGT program.[19]

III. RESULTS AND DISCUSSION

A. Structural characterization

In these studies, the crystalline nature of the ZnO samples remained constant throughout the study. For example, Fig. 1 shows XRD characterization (2θ—intensity scan) of as-deposited (T_{dep} = 750 °C, $pO_2 = 10^{-5}$ Torr) and laser-irradiated ZnO thin films with 20 and 40 pulses of laser output energy density of 200 mJ/cm^2. The XRD pattern shows that the films are highly textured or epitaxial with a *c*-axis preferred orientation. No substantial change in (002) diffraction peak intensity and full width at half maximum (FWHM) was observed in the laser-irradiated

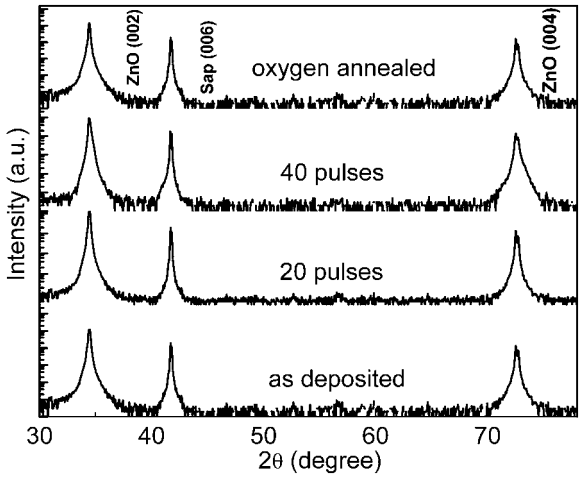


FIG. 1. Room temperature x-ray diffraction pattern of as-deposited, laser-irradiated, and oxygen-annealed films.

https://doi.org/10.1557/jmr.2011.74 Published online by Cambridge University Press

ZnO thin films, indicating good crystalline quality of the films even after irradiation with 40 laser pulses. Within the detection limit of the XRD apparatus, there was no evidence of precipitation or impurity clustering in the films following laser irradiation.

Figure 2 displays the XRD patterns of the ZnO (002) peak for the as-grown (T_{dep} = 350 °C, $pO_2 = 10^{-6}$ Torr) and the oxygen-annealed (up to 800 °C for 30 min.) films. In the annealed sample, the angular position of ZnO (002) peak shifts toward $2\theta = 34.44°$ (ZnO_{bulk}), indicating the relaxation of stress that occurs in high temperature oxygen-annealed samples. The FWHM decreases nearly linearly with increasing annealing temperature. Above 500 °C, the "*c*" lattice parameter of ZnO decreases with increasing temperature as revealed by the shift of ZnO (002) peak toward higher values. We believe that significant oxygen diffusion occurs in these samples above ~500 °C.[20] High temperature thermal annealing in oxygen environment leads to higher atomic mobility and oxygen diffusion into the film and hence to a reduction in the concentration of intrinsic point defects (V_O and I_{Zn}) and compressive stress originating from them. To summarize, thermal annealing in oxygen atmosphere leads to (i) an increase in intensity of ZnO (002) reflection, (ii) decrease in FWHM, and (iii) relaxation of intrinsic residual stress.

A detailed TEM study was performed to investigate the microstructure and verify the epitaxial relationship of the as-grown and laser-irradiated films. The low magnification bright-field TEM cross-section micrograph revealed the absence of any precipitates or clustering in the irradiated films (figure not shown). The high-resolution TEM micrograph [Fig. 3(a)], which is representative of the entire sample, reveals the highly epitaxial nature of the film and the atomically sharp interface with no evidence of any interfacial reaction or precipitation. The thickness of the film was determined to be around 650 nm. Both the fast Fourier transformation and the selected area diffraction pattern [Fig. 3(b)] show spots corresponding exclusively to the film and substrate. The detailed XRD and the TEM analyses suggest that laser irradiation with 40 pulses did not alter the crystalline quality substantially or result in precipitation and cluster formation in the ZnO films.

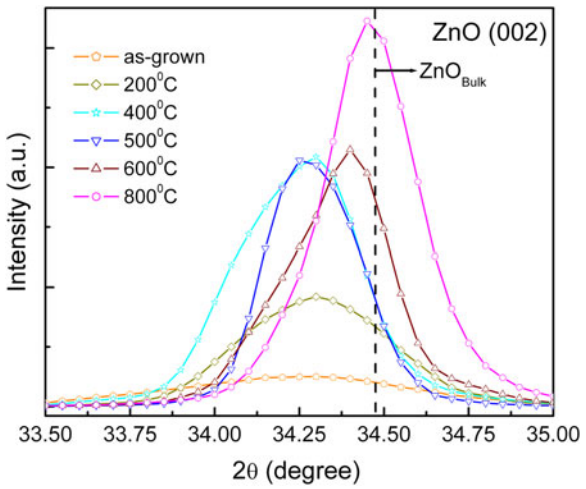


FIG. 2. ZnO (002) peak position of the films annealed in oxygen atmosphere at different temperatures.

B. Magnetic and transport studies

Magnetic and transport measurements were performed on as-grown ZnO thin film samples prepared under different growth conditions and annealed in different atmosphere. Figure 4 shows the room temperature magnetization data plotted as a function of the applied magnetic field for ZnO films grown (i) at different T_{dep} and (ii) under different pO_2. It can be seen from Fig. 4 that saturation magnetization (M_s) decreases with an increase in the T_{dep} and pO_2. ZnO films grown in different pO_2 and at different T_{dep} showed coercivity values in the range of 59–219 Oe; the highest coercivity (~219 Oe) was observed in the films grown at 650 °C and 10^{-3} Torr pO_2. Table I summarizes the important parameters, such as, ρ (mΩ-cm), *n* (/cm^3), and μ (cm^2/V·s) of the samples grown at different T_{dep} and different pO_2. Polycrystalline ZnO films grown at room temperature and pO_2 of 10^{-6} Torr had the highest carrier concentration of $\sim 2.2 \times 10^{20}$ cm^{-3}. It is clear from the dependency of *n* on both T_{dep} and pO_2 that lowering the T_{dep} is a more effective way of achieving higher n-type carrier concentrations. Resistivity gradually increases from 9.44 to 41.7 mΩ-cm as the T_{dep} is increased from 27 to 750 °C. It also increases by three orders of magnitude (from 14.4 to 13,860 mΩ-cm) as the pO_2 increases from 10^{-6} to 1 Torr, suggesting a strong dependence on pO_2.

Figure 5 demonstrates the hysteresis (M–H) loops of the ZnO films annealed at different temperatures under oxygen atmosphere (760 Torr). It is clear from the plot that there is a gradual reduction in the magnetization value from ~1 emu/cm^3 (as-grown) as the annealing temperature is increased from 200 to 800 °C. As expected, longer anneals result in lower M_s values, e.g., the M_s for the sample annealed at 500 °C for 4 h is lower than the sample annealed for 30 min. Finally, when the films were annealed at temperatures 600 °C or higher they turn out to be diamagnetic. Figure 6 shows plots of carrier concentration and resistivity of ZnO films versus the annealing temperature. Annealing at up to 600 °C results in a modest change in the electrical properties (e.g., *n* decreased to $\sim 3.42 \times 10^{19}$cm^{-3} and ρ increased to ~18.3 mΩ-cm), whereas a dramatic change ($n \sim 10^{15}$ and ρ ~870 Ω-cm) is observed after annealing at 800 °C. This change in electrical properties is consistent with the shift of the (002) ZnO peak toward a higher angle, as revealed in the XRD patterns (Fig. 2). It is important to note that films annealed at 600 °C for 30 min still exhibit a high carrier

https://doi.org/10.1557/jmr.2011.74 Published online by Cambridge University Press

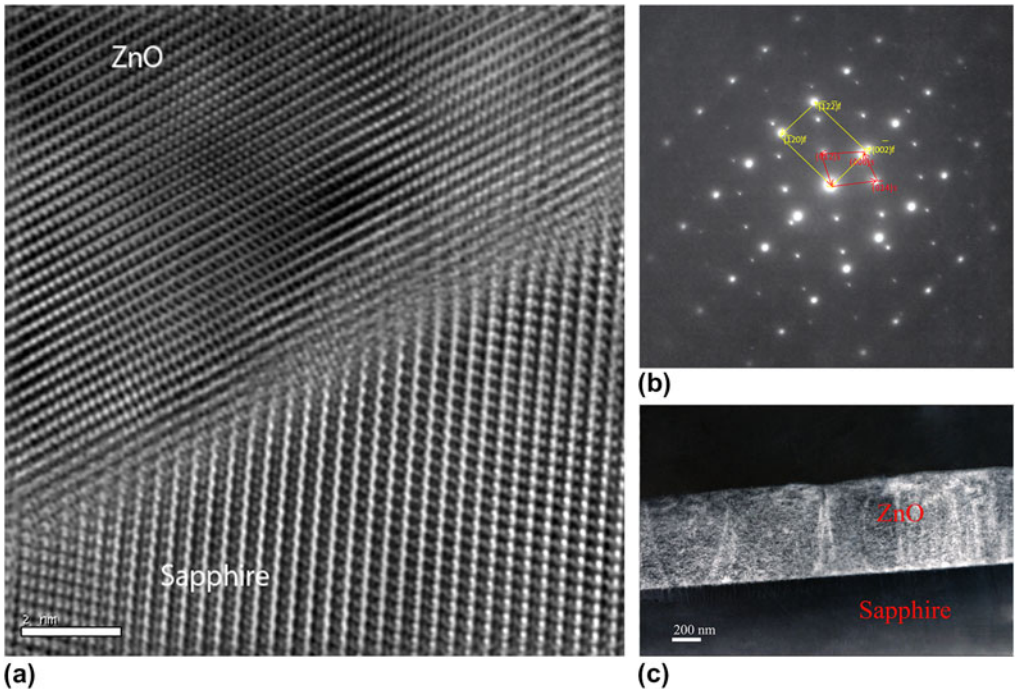


FIG. 3. (a) Fourier-filtered high-resolution transmission electron microscope image of laser-irradiated ZnO (tilted to [$\bar{2}$110] zone) showing highly epitaxial film on sapphire with an atomically sharp interface. (b) Indexed selected area diffraction pattern of film/substrate interface. (c) Bright-field image of the film showing the film thickness.

concentration of ~3.4 × 10^{19} cm^{-3}, although no ferromagnetism was observed in these films. Likewise, the temperature-dependent Hall measurements[21] on an as-grown sample (T_{dep} = 380 °C and pO_2 = 200 Torr) show that the carrier concentration drops from ~9 × 10^{17} cm^{-3} (300 K) to ~10^{15} cm^{-3} (10 K), whereas M_s of undoped ZnO (T_{dep} = 350 °C and pO_2 = 10^{-6} Torr) increases only marginally with the decrease in temperature (Fig. 7), as is typical of ferromagnetic behavior. The lack of direct correlation between carrier concentration and magnetic moment leads us to conclude that carrier-mediated ferromagnetism does not appear to be the active exchange mechanism operating in the undoped ZnO system.

The absence of any correlation between carrier concentration and magnetic moment was clearly demonstrated in some of our earlier studies where we had examined the RTFM of (Cu, Al):ZnO[22] systems. All the epitaxial-doped ZnO films showed ferromagnetic ordering at room temperature. The moment increased with increasing Cu concentration up to 5%. The 2% Cu sample had a total moment of 7 emu/cm^3; 5% Cu sample had a total moment of 14 emu/cm^3; and the 10% had a total moment of 10.5 emu/cm^3. The drop in moment at highest Cu concentration could be due to an increased occurrence of antiferromagnetic coupling between Cu pairs occurring at shorter separation distances, which had been predicted in earlier theoretical studies.[23] The presence of Cu ions in ZnO increases the resistivity up to three orders. The resistivity of undoped ZnO is about 10–20 mΩ-cm and that of the $Zn_{1-x}Cu_xO$ films is of the order of 10 Ω-cm. Codoping the Cu:ZnO thin films with Al, an extrinsic donor, then leads to a large increase in the free carrier concentration. Al in +3 state behaves as a donor in ZnO and hence introduces carriers in the form of electrons. For example, for the 2% Cu-doped ZnO samples, the room temperature Hall measurements show that the electron concentration can be increased from 1.0 × 10^{17} to 1.5 × 10^{20} by increasing Al concentration up to 5% Al. Further increase in Al content leads to a decrease in both sample conductivity and carrier density. Interestingly, an increase in carrier density of three orders of magnitude to 10^{20} cm^{-3} does not improve the ferromagnetism. Even though the role of free carriers cannot be entirely ruled out as the 2% Cu-doped ZnO still has a carrier concentration of 10^{17} cm^{-3}, defects associated with oxygen-deficient compositions (e.g., V_O) appear to be having a much greater effect in mediating ferromagnetic ordering in this ZnO-based DMS system. This further reinforces our belief that a free carrier-mediated mechanism (e.g., Ruderman-Kittel-Kasuya-Yosida (RKKY) or double exchange) is not a plausible explanation for ferromagnetism in ZnO-based DMS materials, and that a defect-mediated mechanism needs to be invoked.

C. Reversible ferromagnetism in ZnO

1. Annealing treatment

The effect of vacuum annealing on RTFM was further explored to extend our investigation to understand the role of defects in controlling the ferromagnetism in our

https://doi.org/10.1557/jmr.2011.74 Published online by Cambridge University Press

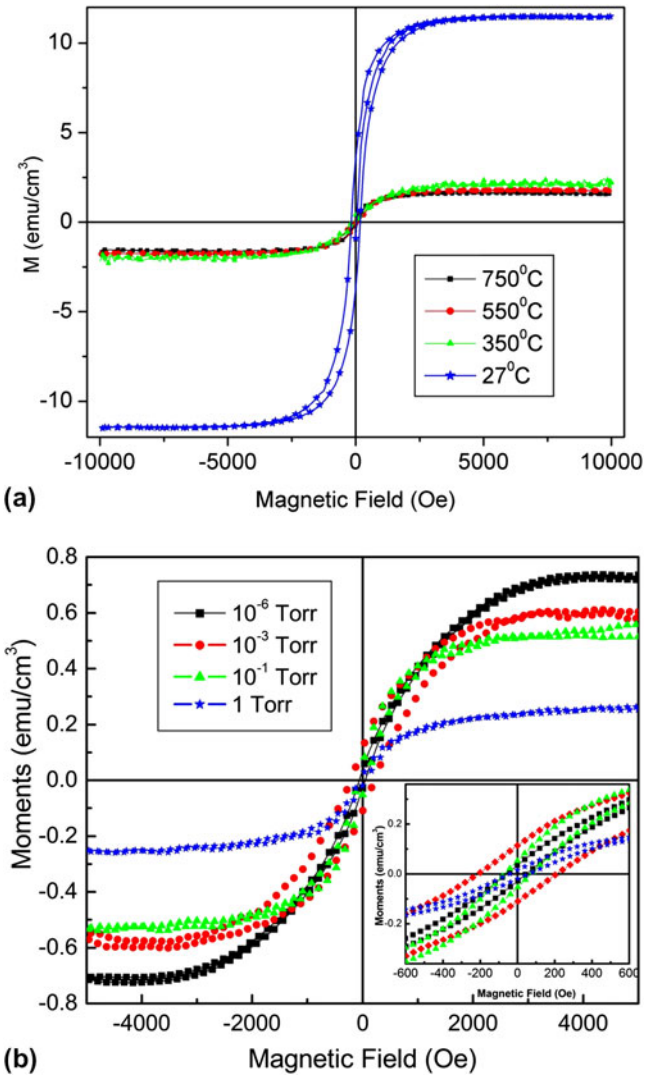


FIG. 4. Room temperature M–H hysteresis curves of ZnO films grown at (a) different substrate temperatures under 10^{-5} Torr; (b) different oxygen partial pressures (pO_2) at 650 °C.

undoped ZnO films. As-grown ZnO films were annealed in vacuum (10^{-5} Torr) at different temperatures for 3 h. As shown in Fig. 8, the M_s gradually increases when the annealing temperature is increased. Figure 9 shows a schematic of the reversible room temperature ferromagnetic ordering in the samples. The inset shows the room temperature hysteresis loops of the samples. As illustrated by this figure, RTFM can be controlled to switch between the "on" and "off" states reproducibly. For example, the RTFM found in as-grown films represents an "on" state that can be converted to the "off" (diamagnetic) state by oxygen annealing at 800 °C for 30 min. Finally, the "on" state can be restored by further vacuum annealing of the previously oxygen-annealed samples. It is important to point out here that the same sample has been used in the oxygen annealing and further vacuum annealing experiments and that the results have been reproduced multiple

TABLE I. Resistivity, carrier concentrations, and mobility of ZnO films grown at different T_{dep} under 10^{-5} Torr pO_2 and under different pO_2 at 650 °C.

		ρ (mΩ-cm)	n (/cm^3)	μ (cm^2/V·s)
T_{dep} (°C) ($pO_2 = 10^{-5}$ Torr)	27	9.44	2.2E20	2.90
	350	11.60	9.0E19	6.00
	550	24.01	3.6E19	7.12
	750	41.70	1.0E19	14.96
pO_2 (Torr) (T_{dep} = 650 °C)	10^{-6}	14.40	5.7E19	7.56
	10^{-3}	18.80	2.1E19	16.10
	10^{-1}	451.00	6.3E17	22.00
	1.0	13,860	1.6E16	28.69

pO_2, oxygen partial pressure.

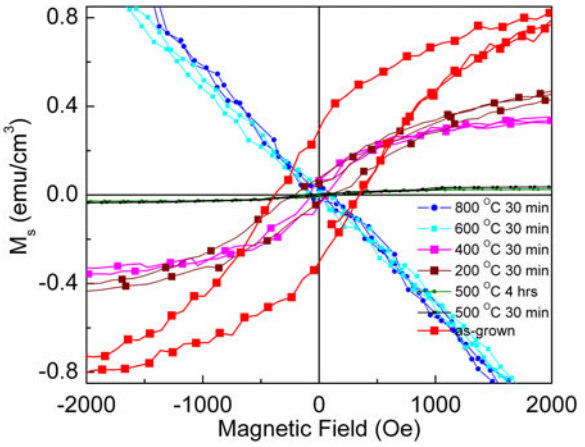


FIG. 5. M–H plot of as-grown (T_{dep} = 650 °C, $pO_2 = 10^{-5}$ Torr) and oxygen-annealed samples at different temperatures.

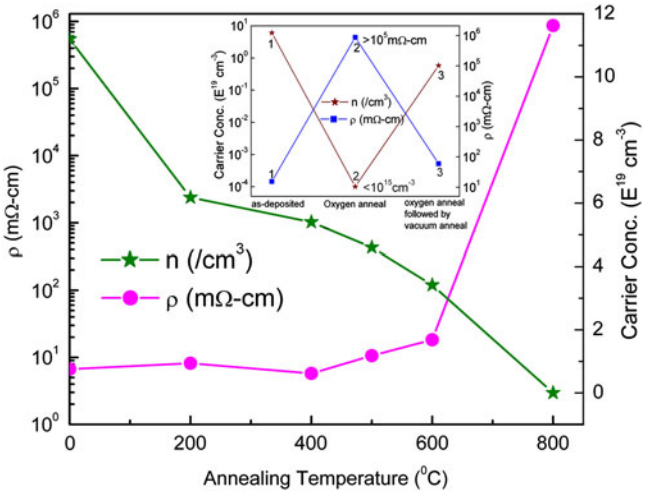


FIG. 6. Carrier concentrations and resistivity of ZnO films annealed at different temperatures in 760 Torr oxygen atmosphere. Inset represents a schematic of the "on" and "off" states of the samples.

times. Vacuum annealing results in an increase in the carrier concentration from ~10^{15} to ~5 × 10^{18} and a decrease in ρ from ~870 to ~60 mΩ-cm. This is likely to be attributed to incorporation of the shallow donor level

https://doi.org/10.1557/jmr.2011.74 Published online by Cambridge University Press

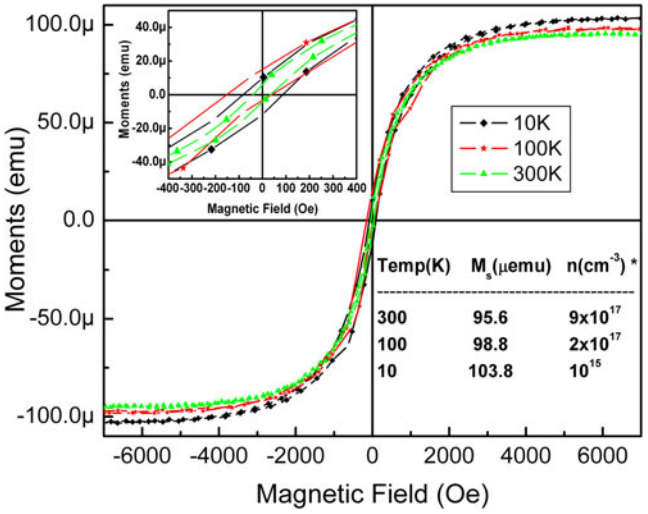


FIG. 7. M–H hysteresis loops of as-grown sample (T_{dep} = 350 °C, $pO_2 = 10^{-5}$ Torr) measured at different temperatures in the range of 300–10 K. [*data (*n*) has been taken from Ref. 21]

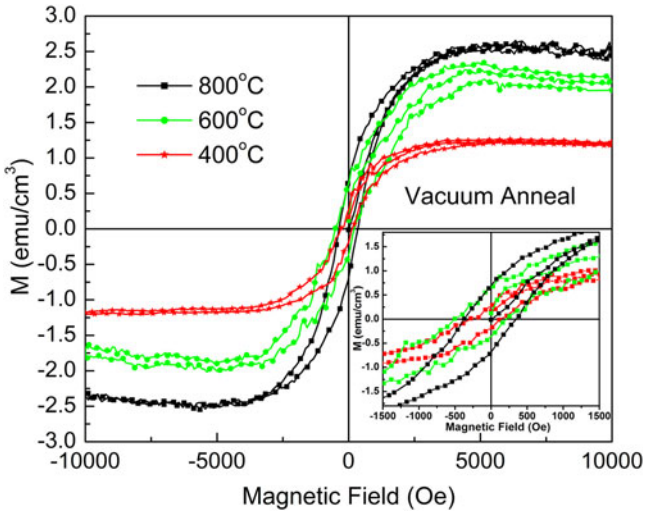


FIG. 8. Room temperature magnetization curves of the vacuum (10^{-5} Torr)-annealed samples at different temperatures.

induced by V_O and/or V_O–I_{zn} pair. It may be recalled here that the inset of Fig. 6 depicts the three states of samples. While "2" represents the "off" state (oxygen annealed at 800 °C and 760 Torr for 30 min), "1" and "3" represent the "on" state (as-grown at 550 °C and 10^{-5} Torr and oxygen annealing at 800 °C followed by vacuum annealing at 850 °C, respectively) of the ZnO films.

The oxygen content in the films has been characterized by XPS studies. An XPS survey spectra (5–1200 eV) and high-resolution scan for Zn and O were performed for the as-grown (T_{dep} = 650 °C, $pO_2 = 10^{-5}$ Torr) and oxygen-annealed (800 °C, 760 Torr, 30 min) samples. The samples were etched by 5 kV Ar^+ ion bombardment for 10 min before the survey scan. The C 1s peak at 285.0 eV was used for calibration. The binding energy of $2p_{3/2}$ (~1022 eV) and

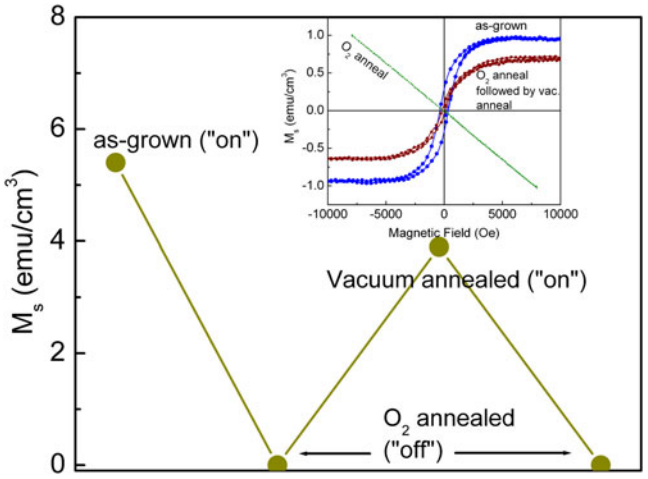


FIG. 9. Schematic plot of the "on" and "off" magnetic states of as-grown, oxygen-annealed, and oxygen annealed followed by vacuum-annealed ZnO films. The inset shows the room temperature hysteresis loops of the same samples.

$2p_{1/2}$ (~1045 eV) levels of Zn corresponding to Zn–O bonding exhibited very similar features before and after oxygen annealing. Figure 10 shows the high-resolution scan of O 1s peak. The peak at ~530 eV has been attributed previously to O^{2-} ions in the stoichiometric wurtzite structure.[24,25] The higher binding energy at ~531.5 eV is associated with O^{2-} ions in oxygen-deficient regions. An electron charge density in the region of a V_O is reduced, which results in less screening of the O^{2-}:1s electrons from their nucleus, thus raising the effective nuclear charge and hence binding energy of an O^{2-}:1s electron.[26] Therefore, the intensity of this component of O 1s peak is associated with the concentration of V_O. It can be clearly seen from Fig. 10 that the intensity of 531.5 eV O 1s peak is significantly reduced in the oxygen-annealed films. Thus, oxygen annealing at a high temperature (800 °C, 30 min) promotes the diffusion of oxygen into the film and leads to a reduction in the concentration of V_O, resulting in a more stoichiometric film.

2. Laser irradiation treatment

We have also investigated the role of low energy pulsed laser irradiation on magnetic properties. Magnetic measurements were performed for all the films in the temperature range 100–300 K and in magnetic fields up to 10 kOe. Figure 11 shows isothermal magnetization data plotted as a function of the applied magnetic field for both the as-deposited and the laser-irradiated films exposed to a series of laser pulses. The diamagnetic contribution from the sapphire substrate has been subtracted using the high-field slope between 5 and 10 kOe. Films deposited at high temperature (750 °C) and under high oxygen pressure of 10^{-2} Torr show a weak ferromagnetic coupling with a small coercive field, H_c (~56 Oe), and a small M_s

https://doi.org/10.1557/jmr.2011.74 Published online by Cambridge University Press

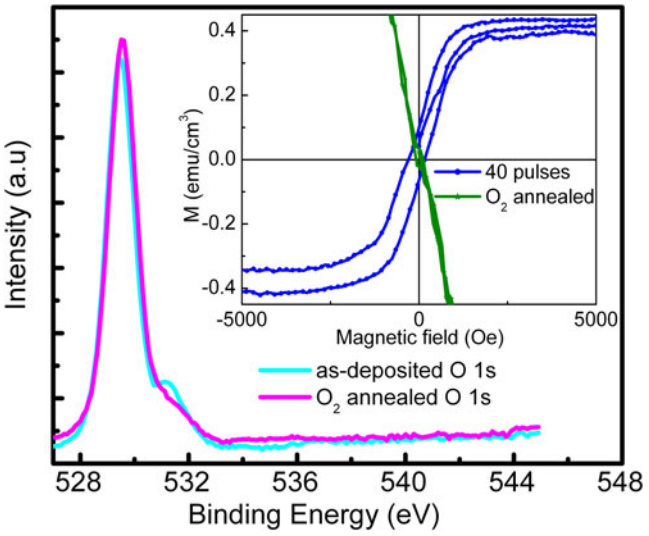


FIG. 10. X-ray photoelectron spectroscopy high-resolution scan of oxygen 1s peak for as-deposited (T_{dep} = 650 °C, $pO_2 = 10^{-5}$ Torr) and oxygen-annealed (at 760 Torr, 30 min) films. The inset shows the room temperature magnetization curve of oxygen-annealed and oxygen annealed followed by laser-irradiated samples.

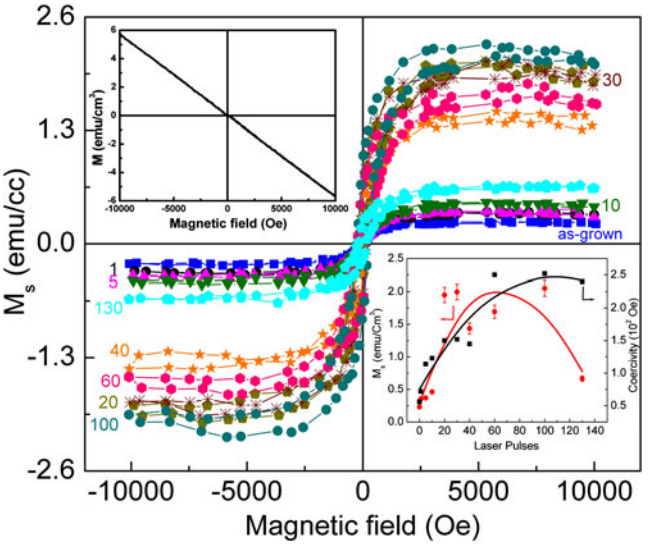


FIG. 11. Room temperature magnetization curves of pure ZnO films irradiated with different number of laser pulses, viz., as-grown, 1, 5, 10, 20, 30, 40, 60, 100, and 130 at 200 mJ/cm^2. Inset (top left) shows diamagnetic behavior of laser-irradiated samples after annealing in O_2 at 800 °C. Inset (bottom right) is the variation of room temperature saturation magnetic moment and coercivity with laser pulses. The solid (red) line represents the generic trend of the variation of magnetization as a function of laser pulses.

(0.2308 emu/cm^3). As shown in the lower right inset of Fig. 11, the M_s of the films increases following laser irradiation due to the simultaneous formation of several defects, such as V_{Zn}, V_O, and their interstitials. Both M_s and H_c increase with the increase in number of laser pulses up to ~30 pulses where the M_s saturates while the coercivity continues to increase up to 130 pulses. A plateau or possible decrease in M_s was observed beyond 100 pulses, which could be attributed to the clustering of newly generated defects accompanied by a concomitant decrease in defect concentrations. Once the defects are in the form of clusters such as dislocation loop, they may lose their magnetic contribution. The M_s, however, increases only marginally with decreasing temperature down to 100 K, suggesting that the Curie temperature is well above 300 K. The magnetization for all the samples saturates at fields of ~3000 Oe. These ferromagnetic ZnO films switched to a perfect diamagnetic state after annealing in oxygen ambient for 20 min at 800 °C, as shown in the top left inset of Fig. 11. Ferromagnetic ordering could again be restored in the oxygen-annealed samples, but only after laser irradiation with 40 pulses. The inset of Fig. 10 shows the room temperature magnetization curve for an oxygen-annealed sample and an oxygen-annealed sample that had then been laser irradiated. It should be pointed out that after irradiating the sample with 20 pulses the magnetization curve appeared very noisy and weak, but 40 laser pulses gave rise to a saturation moment of 0.42 emu/cm^3, which is higher than the 0.3 emu/cm^3 moment of the as-deposited film. The laser irradiation treatment also restored the carrier concentration in oxygen-annealed samples. After an O_2 anneal at 800 °C for 20 min, the carrier concentration had dropped significantly to ~10^{14}/cm^3, but then rises to ~10^{19}/cm^3 after an exposure to 40 laser pulses.

D. Defect characterization and phenomenological model

In our SIMS and EELS studies, we ruled out the possibility of ferromagnetic contamination as being responsible for the observed RTFM. Figure 12 shows the EELS spectra of the as-grown sample (T_{dep} = 650 °C, $pO_2 = 10^{-5}$ Torr) in the range of 400–1300 eV. In the higher energy loss region, the only observed edges are that of the oxygen K-edge at ~532 eV and the zinc $L_{2,3}$-edges at ~1020 and 1043 eV, respectively. No magnetic impurity was found within the detection limit of the EELS. The inset of Fig. 12 shows the depth profile of impurity concentration of as-grown ZnO films. Upon comparing with the standards, we found that the Fe concentration was about 1 ppm and that the Ni, Co, Mn concentrations were lower than that of Fe. It is important to note that EELS and SIMS studies revealed similar impurity levels in the oxygen-annealed and laser-irradiated samples. The lowest saturation moment of 0.2308 emu/cm^3 was observed in the film grown at 750 °C in 10^{-2} Torr pO_2. This moment would correspond to a concentration of 4.1×10^{18} atoms/cm^3 of a ferromagnetic impurity having a moment of 6 μ_B/atom. SIMS study revealed that Fe contamination was at a concentration level of 1 ppm, which is two orders of magnitude below the above critical value. Oxygen-annealed samples also had the same amount of Fe contamination, but they did not show any ferromagnetism

https://doi.org/10.1557/jmr.2011.74 Published online by Cambridge University Press

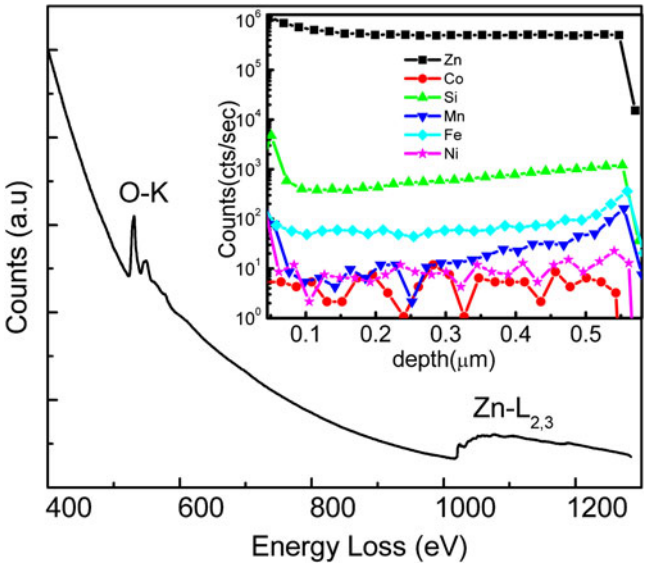


FIG. 12. Electron energy loss spectrometer spectra of as-grown (T_{dep} = 650 °C, $pO_2 = 10^{-5}$ Torr) ZnO film. Inset shows the secondary ion mass spectrometer depth profile of Co, Si, Mn, Fe, and Ni impurities in as-grown (T_{dep} = 650 °C, $pO_2 = 10^{-5}$ Torr) ZnO films.

down to 10 K. Coey[27] pointed out that iron could be diffusing from the substrate holder into the sapphire at high temperature (700 °C) and forming ferromagnetic nanoparticle precipitates, giving rise to RTFM. In our case, a very high saturation moment (11.5 emu/cm^3) was observed in the polycrystalline samples grown at room temperature, where one would not expect any diffusion of iron into the sapphire. In addition, the x-ray and TEM studies provided no evidence for the presence of magnetic precipitates in the ZnO films. These results clearly rule out the possibility of any external ferromagnetic contamination and establish the fact that the observed ferromagnetism must be defect mediated rather than impurity induced.

The nature of the defects responsible for conductivity and ferromagnetism in our undoped ZnO films can be established as follows. The creation and destruction of point defects in semiconducting oxide films are governed by a thermodynamic equilibrium in the postgrowth annealing. Annealing in oxygen atmosphere definitely reduces the population of V_O, whereas annealing in vacuum (10^{-5} Torr) may create both V_{Zn} and V_O. As mentioned earlier, the very high formation energy of I_{Zn} in n-type ZnO[28] (~4 eV) prevents their formation in the vacuum (10^{-5} Torr)-annealed samples. Further, it is well known that V_{Zn} are acceptors and give rise to the p-type conductivity. Since our samples continue to show the n-type conductivity after vacuum annealing, we are inclined to suggest that the vacuum annealing creates V_O that act as a source of the n-type conductivity and ferromagnetism (assuming singly charged V_O). The nature of defects which causes the intrinsic n-type characteristics has been widely debated in the literature recently.[29–31] V_O, Zn_i, and their complexes are theoretically considered to be the sources of n-type conductivity in ZnO[29], although only the V_O–I_{Zn} complex is predicted to be present as a shallow donor under oxygen-deficient conditions. The highly mobile nature of oxygen and I_{Zn}[32] also suggests that the oxygen interstitials will migrate rather quickly to the surface and be emitted. Since laser irradiation was performed in ambient atmosphere, the I_{Zn} will also be oxidized as soon as they reach out to the surface. All the above-presented arguments suggest that the n-type behavior in our studies is a result of a V_O–I_{Zn} complex formation.

To further understand the local environment of the point defects present in the as-grown and annealed ZnO films, we used x-band (~9.5 GHz) EPR spectroscopy on a set of samples grown and treated under conditions. The experiments were carried out by applying external magnetic field H both parallel and perpendicular to the film c-axis in the temperature range of 4–300 K.

Figures 13(a)–13(d) show typical experimental EPR spectra (T = 4 K) of as-grown and annealed ZnO films in various environments for the $H \parallel c$-axis orientation. The observed spectral components for both H parallel and perpendicular to the c-axis are as follows. (i) A prominent broad peak (ΔH_{pp} ~80 G, g ~2) was observed for all the samples except for the oxygen-annealed ZnO. This signal is attributed to the point defects in the ZnO films and here onwards it is referred to as the "ZnO signal." (ii) Six sharp lines, overlapping the ZnO signal, correspond to the Mn^{2+} (with electronic spin S = 5/2 and nuclear spin I = 5/2) impurities. While the six lines correspond to the central $|M_S = -1/2\rangle \rightarrow |M_S = +1/2\rangle$ ($\Delta M_I = 0$) hyperfine transition, the less intense intermediary sets of the lines are due to the forbidden nuclear spin transitions, i.e., $\Delta M_I = \pm 1$. (iii) The hyperfine coupling constant $A = 80 \pm 2$ Oe is same for the both film orientations studied, i.e., $H \parallel$ and $\perp$ to c-axis, indicating that the Mn^{2+} ions are in a high symmetry environment. (iv) The additional clusters of six lines flanking the intense central six lines correspond to the $|M_S = -3/2\rangle \rightarrow |M_S = -1/2\rangle$ and $|M_S = +1/2\rangle \rightarrow |M_S = +3/2\rangle$ ($\Delta M_I = 0$) transitions. The zero-field splitting parameter $|D|$ can then be estimated as ~225 ± 10 Oe. The observed D and A values for Mn^{2+} in our ZnO films are in agreement with other systems containing Mn^{2+} as either an impurity or a dopant.[33,34]

The surprising prominent varying intensities of the Mn^{2+} spectrum with respect to the ZnO signal in our samples could be due to a combination of various factors such as EPR cavity quality (Q) factor that was varied due to different dielectric losses in the partially conductive sample, microwave power at the sample site, and/or other changes in the experimental configuration. However, despite its prominence, the integrated area under the Mn^{2+} EPR peak is significantly smaller (by a factor of ~10^3) than that of the ZnO signal in all the samples. The

https://doi.org/10.1557/jmr.2011.74 Published online by Cambridge University Press

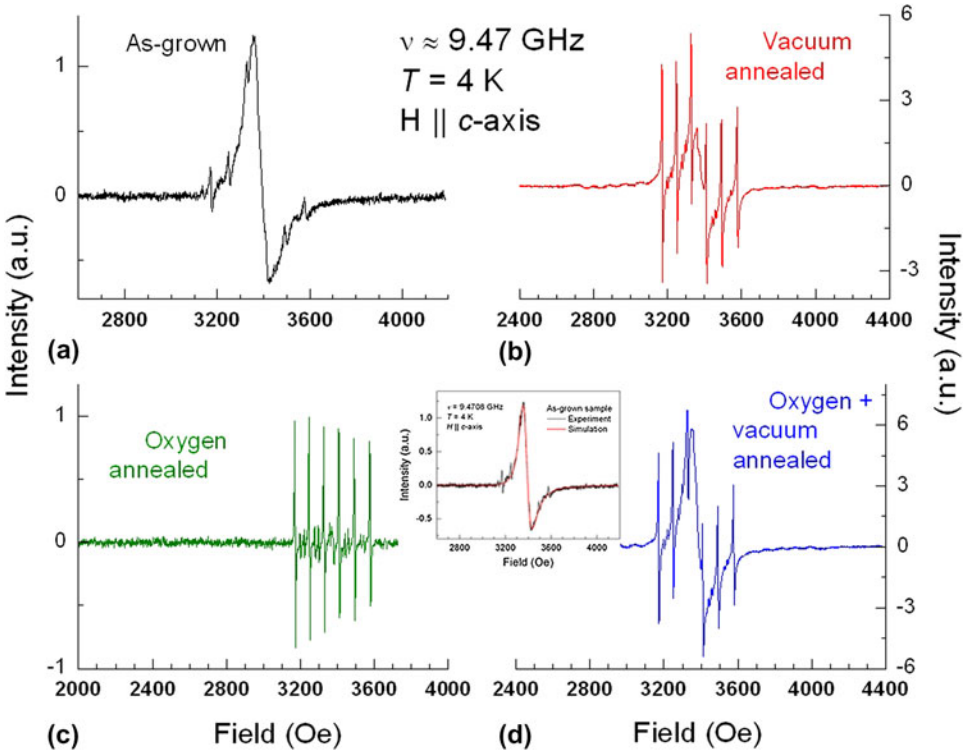


FIG. 13. Experimental x-band electron paramagnetic resonance spectra of ZnO films grown and treated under the conditions (a) As-grown, (b) annealed in vacuum, (c) annealed in the presence of oxygen, and (d) oxygen followed by vacuum annealing. The inset shows the experimental (black) and least square fit (red) spectra of as-grown ZnO shown in (a). The fit is done using EWVOIGT program[19] with the parameters: Lorentzian line shape, $g = 1.997$ and $\Delta H_{pp} = 78$ G.

Mn^{2+} represents a minor impurity and the rest of the discussion will focus only on the ZnO signal.

Annealing of the as-grown films in presence of oxygen resulted in a complete disappearance of the ZnO EPR signal [Fig. 13(c)]. However, the ZnO signal reappears upon subsequent vacuum annealing of the films [Fig. 13(d)]. These observations are fully consistent with the "on" and "off" behavior observed in the magnetization and the changes in conductivity of the ZnO films. This indicates that the spins that are responsible for the magnetism in these ZnO films could be the same as those being directly observed by EPR.

The electronic g-factors and peak-to-peak line widths (ΔH_{pp}) of the ZnO signal in all the samples studied were obtained by performing a nonlinear least squares fitting of the experimental spectra (see inset of Fig. 13) using the EWVOIGT program[19] and a Lorentzian line shape model that includes a variable dispersion contribution. The admixture of dispersion was found to be essential for accounting for the observed line shape, which is attributed to a shift of the microwave phase within the conductive ZnO film (i.e., skin depth effects are responsible for the signal asymmetry that is known as a Dysonian line shape[35]).

Comparison of the literature data on EPR of the single crystal ZnO with our EPR results is useful. But it must be emphasized that most of the reported EPR studies in the literature used single crystal ZnO samples either pristine[36,37] or irradiated by high energy electrons.[36–43] In contrast, our samples were thin films (~700-nm thick) and not subjected to any electron irradiation. Also, EPR spectra from our samples were observed without any in situ illumination by 325–515-nm light used in the earlier studies.[36–43] Even though the nature of our ZnO samples and the EPR experimental conditions were quite different than those of the previous studies,[36–43] it is worthwhile to highlight and compare the major features of the observed signals. First, for the ZnO films studied in this study both the dominating ZnO and the minor Mn^{2+} impurity signals vanished beyond the EPR detection limit at temperatures above 40 K. In contrast, the EPR signals from ZnO crystals have been reported at temperatures as high as 90 K.[36–43] Although this could be attributed to a higher spin count in larger crystals versus thin films, the differences in electronic relaxation mechanisms would be another possible explanation. Second, the ZnO EPR signals reported in the literature[36–43] were as narrow as 2–6 G, while ΔH_{pp} of the EPR lines in our samples were 70–95 G. We speculate that the larger line width in our samples could be due to a combination of inherent strains (e.g., lattice mismatch with respect to the substrate) present in the film, a faster relaxation of the unpaired spins due to the interaction with the Mn^{2+} impurity, and finally additional magnetic

https://doi.org/10.1557/jmr.2011.74 Published online by Cambridge University Press

interactions (both dipolar and spin exchange) with the different point defects.

The observed g values of the ZnO line observed in our studies of this film lie in between the reported g-values for V_O ($g_{iso} \sim 1.996$)[39–42] and V_{Zn} ($g_{iso} \sim 2.013$)[38,42,43] in the ZnO crystals and, therefore, the exact nature of the point defects in the ZnO thin films cannot be ascertained by the EPR data alone. However, combining EPR results with the magnetization and conductivity data, we tentatively assign the observed ZnO peak, with $g_{iso} = 2.00$–2.01 to the V_O.

IV. CONCLUSIONS

In summary, we have systematically studied the structural, chemical, electrical, and magnetic properties of undoped ZnO thin films grown on c-sapphire by PLD under different growth conditions and annealed in different atmosphere. The magnetic properties of the nominally pure ZnO samples have been found to depend strongly on processing conditions and postgrowth annealing treatments. TEM studies have ruled out the presence of any magnetic precipitates and second phases as the source of the magnetism. SIMS and EELS analyses indicated that TM contamination (Fe and Mn with lesser amounts of Ni and Co) in the pure ZnO samples were below 10 ppm. We have found that ferromagnetism is always correlated with conditions that results in films that are substoichiometric in oxygen, while stoichiometric ZnO films always tend toward diamagnetism. Here, we have successfully demonstrated reproducible switching between "off" and "on" ferromagnetic states using oxygen annealing in combination with either laser irradiation or vacuum annealing treatments. High temperature annealing in oxygen brings the films to near-stoichiometric conditions and appears to relax the intrinsic residual stress resulting from the presence of point defects. A suspected decrease of V_O upon oxygen annealing has been confirmed in our own XPS studies. Detailed room temperature Hall measurements reveal that the resistivity and carrier concentration of undoped films also vary with growth conditions and can be switched "off" and "on" by using high temperature oxygen annealing and further vacuum annealing, respectively. But, studies on the TM-doped samples have shown that magnetism does not correlate with neither resistivity nor carrier concentration. Three orders of magnitude variations in both resistivity and carrier concentration can be realized without significantly altering the magnetic properties of the sample. As already indicated, we have discovered that pulsed laser irradiation at low laser energy densities, just below the level where melting occurs, can be an effective way of introducing defects into ZnO that lead to RTFM. This would appear to provide a means of patterning ZnO surfaces with magnetic and diamagnetic features. The magnetic moment increases with the number of laser pulses up to about 40 hits and then saturates and/or begins to tail off. The laser-irradiated samples also show a significant increase in n-type electrical conductivity and an increase in free carrier concentration. The induced ferromagnetism can be reversed upon thermal annealing in pure oxygen. We believe that nanosecond laser irradiation introduces a large population of vacancies (particularly V_O) and dangling bonds. These in turn introduce donor states that explain the increase in free carrier densities and unpaired electrons (e.g., electron spins in oxygen atoms in tetrahedron sites around V_{Zn}) that introduce localized magnetic moments.

EPR measurements indicate the presence of a broad peak at $g = 2.01$. This would be most consistent with the magnetic moment arising from the V_O ($g = 1.996$), although the possible contribution from V_{Zn} ($g = 2.013$) cannot be entirely ruled out. We believe that the long-range magnetic exchange interaction that leads to the ferromagnetism is actually mediated by the V_O, which form bound magnetic polarons that effectively couple nearby moments. The occurrence of ferromagnetism in some other transparent oxides has been explained by the above-mentioned mechanism.

All these results have clearly established that for ZnO there is a strong correlation between RTFM and presence of trapped nonequilibrium concentrations of defects (vacancies, dangling bonds, and other radiation-induced defects). It is concluded that there exist defect-assisted mechanisms that both introduce magnetic moments and lead to the occurrence of long-range ferromagnetic ordering in ZnO films at room temperature even in the absence of other 3d TM ion dopants. We have forwarded what would seem to be a plausible explanation for this observed behavior. But, we have not been able to conclusively identify the exact defect states that are producing the magnetism in ZnO. However, we have clearly captured the phenomenology and hope that this will help others in the future to finally identify the exact mechanisms that lead to magnetism in both pure and TM-doped ZnO films.

ACKNOWLEDGMENTS

The authors thank Prof. A.I. Smirnov and Dr. S. Nellutla for the EPR measurements. The authors are pleased to acknowledge the support of the Army Research Office under Grant No. W911NF-04-D-0003.

REFERENCES

1. H. Ohno: Making nonmagnetic semiconductor ferromagnetic. *Science* **281**, 951 (1998).
2. T. Dietl: Dilute magnetic semiconductors: Functional ferromagnets. *Nat. Mater.* **2**, 646 (2003).
3. S. Ramachandran, A. Tiwari, and J. Narayan: $Zn_{0.9}Co_{0.1}O$-based diluted magnetic semiconducting thin films. *Appl. Phys. Lett.* **84**, 5255 (2004).
4. K. Ueda, H. Tabata, and T. Kawai: Magnetic and electric properties of transition-metal-doped ZnO films. *Appl. Phys. Lett.* **79**, 988 (2001).

https://doi.org/10.1557/jmr.2011.74 Published online by Cambridge University Press

5. C.N.R. Rao and F.L. Deepak: Absence of ferromagnetism in Mn and Co doped ZnO. *J. Mater. Chem.* **15**, 573 (2005).
6. T.C. Kaspar, T. Droubay, S.M. Heald, P. Nachimuthu, C.M. Wang, V. Shutthanandan, C.A. Johnson, D.R. Gamelin, and S.A. Chambers: Lack of ferromagnetism in n-type cobalt-doped ZnO epitaxial thin films. *New J. Phys.* **10**, 055010 (2008).
7. M. Gacic, G. Jakob, C. Herbort, H. Adrian, T. Tietze, S. Brück, and E. Goering: Magnetism of Co-doped ZnO thin films. *Phys. Rev. B* **75**, 205206 (2007).
8. M. Venkatesan, C.B. Fitzgerald, and J.M.D. Coey: Thin films: Unexpected magnetism in a dielectric oxide. *Nature* **430**, 630 (2004).
9. N.H. Hong, J. Sakai, N. Poirot, and V. Brize: Room-temperature ferromagnetism observed in undoped semiconducting and insulating oxide thin films. *Phys. Rev. B* **73**, 132404 (2006).
10. J.M.D. Coey: d^0 ferromagnetism. *Solid State Sci.* **7**, 660 (2005).
11. D. Kim, J. Hong, Y.R. Park, and K.J. Kim: The origin of oxygen vacancy induced ferromagnetism in undoped TiO_2. *J. Phys. Condens. Matter* **21**, 195405 (2009).
12. A. Sudaresan, R. Bhargavi, N. Rangarajan, U. Siddesh, and C.N.R. Rao: Ferromagnetism as a universal feature of nanoparticles of the otherwise nonmagnetic oxides. *Phys. Rev. B* **74**, 161306(R) (2006).
13. B. Panigrahy, M. Aslam, D.S. Misra, M. Ghosh, and D. Bahadur: Defect-related emissions and magnetization properties of ZnO nanorods. *Adv. Funct. Mater.* **20**, 1161 (2010).
14. G. Xing, D. Wang, J. Yi, L. Yang, M. Gao, M. He, J. Yang, J. Ding, T.C. Sum, and T. Wu: Correlated d^0 ferromagnetism and photoluminescence in undoped ZnO nanowires. *Appl. Phys. Lett.* **96**, 112511 (2010).
15. M. Kapilashrami, J. Xu, V. Strom, K.V. Rao, and L. Belova: Transition from ferromagnetism to diamagnetism in undoped ZnO thin films. *Appl. Phys. Lett.* **95**, 033104 (2009).
16. J. Narayan, S. Nori, D.K. Pandya, D.K. Avasthi, and A.I. Smirnov: Defect dependent ferromagnetism in MgO doped with Ni and Co. *Appl. Phys. Lett.* **93**, 082507 (2008).
17. Q. Wang, Q. Sun, G. Chen, Y. Kawazoe, and P. Jena: Vacancy-induced magnetism in ZnO thin films and nanowires. *Phys. Rev. B* **77**, 205411 (2008).
18. K. Potzger, S. Zhou, J. Grenzer, M. Helm, and J. Fassbender: An easy mechanical way to create ferromagnetic defective ZnO. *Appl. Phys. Lett.* **92**, 182504 (2008).
19. A.I. Smirnov and T.I. Smirnova: High-field ESR spectroscopy in membrane and protein biophysics, in *Biological Magnetic Resonance*, edited by L.J. Berliner and C. Bender (Kluwer, New York, 2004); Vol. 21, pp. 277–348.
20. C. Sudhakar, P. Kharel, G. Lawes, R. Suryanarayanan, R. Naik, and V.M. Naik: Raman spectroscopic studies of oxygen defects in Co-doped ZnO films exhibiting room-temperature ferromagnetism. *J. Phys. Condens. Matter* **19**, 026212 (2007).
21. K.T. Roro, G.H. Kassier, J.K. Dangbegnon, S. Sivaraya, J.E. Westraadt, J.H. Neethling, A.W.R. Leitch, and J.R. Botha: Temperature-dependent Hall effect studies of ZnO thin films grown by metalorganic chemical vapour deposition. *Semicond. Sci. Technol.* **23**, 055021 (2008).
22. D. Chakraborti, G. Trichy, J. Narayan, J.T. Prater, and D. Kumar: Effect of Al doping on the magnetic and electrical properties of Zn (Cu)O based diluted magnetic semiconductors. *J. Appl. Phys.* **102**, 113908 (2007).
23. L.H. Ye, A.J. Freeman, and B. Delley: Half-metallic ferromagnetism in Cu-doped ZnO: Density-functional calculations. *Phys. Rev. B* **73**, 033203 (2006).
24. R. Cebulla, R. Weridt, and K. Ellmer: Al-doped zinc oxide films deposited by simultaneous rf and dc excitation of a magnetron plasma: Relationships between plasma parameters and structural and electrical film properties. *J. Appl. Phys.* **83**, 1087 (1998).
25. L.K. Rao and V. Vinni: Novel mechanism for high speed growth of transparent and conducting tin oxide thin films by spray pyrolysis. *Appl. Phys. Lett.* **63**, 608 (1999).
26. J.C.C. Fan and J.B. Goodenough: X-ray photoemission spectroscopy studies of Sn-doped indium-oxide films. *J. Appl. Phys.* **48**, 3524 (1977).
27. J.M.D. Coey: Dilute magnetic oxides. *Curr. Opin. Solid State Mater. Sci.* **10**, 83 (2006).
28. A. Janotti and C.G. Van de Walle: Fundamentals of zinc oxide as a semiconductor. *Rep. Prog. Phys.* **72**, 126501 (2009).
29. Y.-S. Kim and C.H. Park: Rich variety of defects in ZnO via an attractive interaction between O vacancies and Zn interstitials: Origin of n-type doping. *Phys. Rev. Lett.* **102**, 086403 (2009).
30. K. Jug and V.A. Tikhomirov: Influence of intrinsic defects on the properties of zinc oxide. *J. Comput. Chem.* **29**, 2250 (2008).
31. S. Lany and A. Zunger: Anion vacancies as a source of persistent photoconductivity in II-VI and chalcopyrite semiconductors. *Phys. Rev. B* **72**, 035215 (2005).
32. A. Janotti and C.G. Van de Walle: Native point defects in ZnO. *Phys. Rev. B* **76**, 165202 (2007).
33. A. Abragam and B. Bleaney: *Electron Paramagnetic Resonance of Transition ions* (Dover publications Inc., New York, 1986).
34. V.K. Jain and G. Lehmann: Electron paramagnetic resonance of Mn^{2+} in orthorhombic and higher symmetry crystals. *Phys. Status Solidi B Basic Res.* **159**, 495 (1990).
35. F.J. Dyson: Electron spin resonance absorption in metals. II. Theory of electron diffusion and the skin effect. *Phys. Rev.* **98**, 349 (1955).
36. N.T. Son, I.G. Ivanov, A. Kuznetsov, B.G. Svensson, Q.X. Zhao, M. Willander, N. Morishita, T. Ohshima, H. Itoh, J. Isoya, E. Janzén, and R. Yakimova: Recombination centers in as-grown and electron-irradiated ZnO substrates. *J. Appl. Phys.* **102**, 093504 (2007).
37. X.J. Wang, L.S. Vlasenko, S.J. Pearton, W.M. Chen, and I.A. Buyanova: Oxygen and zinc vacancies in as-grown ZnO single crystals. *J. Phys. D Appl. Phys.* **42**, 175411 (2009).
38. D. Galland and A. Herve: ESR spectra of the zinc vacancy in ZnO. *Phys. Lett.* **33A**, 1 (1970).
39. D.R. Locker and J.M. Meese: Displacement thresholds in ZnO. *IEEE Trans. Nucl. Sci.* **19**, 237 (1972).
40. C. Gonzalez, D. Galland, and A. Herv: Hyperfine interactions of the F^+ center in ZnO. *Phys. Status Solidi B* **72**, 309 (1975).
41. L.S. Vlasenko and G.D. Watkins: Optical detection of electron paramagnetic resonance for intrinsic defects produced in ZnO by 2.5-MeV electron irradiation *in situ* at 4.2 K. *Phys. Rev. B* **72**, 035203 (2005).
42. L.A. Kappers, O.R. Gilliam, S.M. Evans, L.E. Halliburton, and N.C. Giles: EPR and optical study of oxygen and zinc vacancies in electron-irradiated ZnO. *Nucl. Instrum. Methods Phys. Res., B* **266**, 2953 (2008).
43. A.L. Taylor, G. Filipovich, and G.K. Lindeberg: Identification of Cd vacancies in neutron-irradiated CdS by electron paramagnetic resonance. *Solid State Commun.* **8**, 1359 (1970).

https://doi.org/10.1557/jmr.2011.74 Published online by Cambridge University Press